



Theory of field emission from dielectric coated surfaces

Yang Zhou  and Peng Zhang ^{*}*Department of Electrical and Computer Engineering, Michigan State University, East Lansing, Michigan 48824-1226, USA*

(Received 19 October 2020; accepted 14 December 2020; published 30 December 2020)

This paper presents an exact analytical theory for field emission from dielectric coated cathode surfaces, by solving the one-dimensional (1D) Schrödinger equation with a double-triangular potential barrier introduced by the coating. The effects of the cathode material (work function and Fermi energy), dielectric properties (dielectric constant, electron affinity, and thickness), applied dc field strength, and cathode temperature are analyzed in detail. For 1D flat cathode surfaces with coating, it is found that the emission current density can be larger than the uncoated case when the dielectric constant is smaller than a certain value $\epsilon_{\text{diel}}^{\text{th}}$ and the dielectric thickness is larger than the threshold value $d_{\text{th}}[\text{nm}] \approx \epsilon_{\text{diel}} W/eF$ with the dielectric constant $\epsilon_{\text{diel}} < \epsilon_{\text{diel}}^{\text{th}}$, where W is the work function of the cathode material, F the applied dc field, and e the elementary charge. Our quantum model is also compared with a modified Fowler-Nordheim equation for a double barrier, showing qualitatively good agreement. Our study provides insights for designing field emitters with higher efficiency and better stability.

DOI: [10.1103/PhysRevResearch.2.043439](https://doi.org/10.1103/PhysRevResearch.2.043439)

I. INTRODUCTION

Electron field emission [1,2] attracts intensive attention in many applications, such as flat panel display [3–5], electron microscopes [6–8], vacuum microelectronics [9,10], x-ray sources [11], high power microwave sources and amplifiers, and high current cathodes [12–19], for its high efficiency, high brightness, low emittance, and miniaturized device size [20,21]. Field emission is also important to the emerging vacuum nanodevices [22–26]. Common challenges of field emission include the operation requirement of high vacuum condition and current instabilities [27,28]. To overcome these problems, ultrathin coatings, such as graphene, graphene oxide, and zinc oxide [29–32], are fabricated onto the emitter to provide chemical and mechanical protection. Coated emitters are demonstrated to not only have longer current stability, but also smaller turn-on electric field (i.e., field at which the cathode starts appreciable electron emission) and enhanced current emission due to the lowering of the effective potential barrier [30–35]. In addition to the artificially fabricated coatings, native oxides or foreign adsorbates can be easily formed on the surface of the emitter at low vacuum condition [36]. The thin oxide film or the coated dielectric layer on the cathode surface forms a double-layer potential barrier, which strongly influences the field emission properties. The heterostructure in the emission barrier introduced by the coating also has its potential to change the electrons' mean transverse energy behavior that affects beam quality, which makes it an active area for photoinjectors for future x-ray free electron

lasers (XFELs) [37,38]. A modified Fowler-Nordheim equation was constructed to account for the double-barrier field emission scenario [39,40]. However, there is still a lack of systematic analysis on the parametric scaling of field emission from coated surfaces and comprehensive understanding of the interplay of various parameters to optimize the design of coated field emitters.

In this study, we develop a quantum analytical solution for field emission from the dielectric coated cathode surface, by solving the one-dimensional (1D) Schrödinger equation subject to the double barrier introduced by the coating layer. The solution is applicable for arbitrary electric dc field, cathode properties (i.e., work function and Fermi level), and dielectric coating properties (i.e., dielectric constant, electron affinity, and thickness). It includes not only field emission but also thermionic emission, and can be further extended to include photoemission. The model predicts that for 1D flat surfaces, coatings of small dielectric constant and large electron affinity tend to enhance the field emission current, which provides insights for the design of a stable and efficient field emitter.

II. THEORETICAL FORMULATION

The energy diagram for electron emission from a 1D dielectric coated metal surface is shown in Fig. 1. Electrons inside the metal would see a double-triangular potential barrier,

$$V(x) = \begin{cases} 0, & x < 0, \\ V_0 - \chi - eF_{\text{diel}}x, & 0 \leq x < d, \\ V_0 + e(F - F_{\text{diel}})d - eFx, & x \geq d, \end{cases} \quad (1)$$

where $V_0 = W + E_F$, with W and E_F being the work function and Fermi level of the metal, respectively; χ is the electron affinity of the dielectric; e is the positive elementary charge; F is the applied dc electric field in the vacuum; $F_{\text{diel}} = F/\epsilon_{\text{diel}}$ is the dc electric field inside the dielectric with ϵ_{diel} the dielectric

^{*}pz@egr.msu.edu

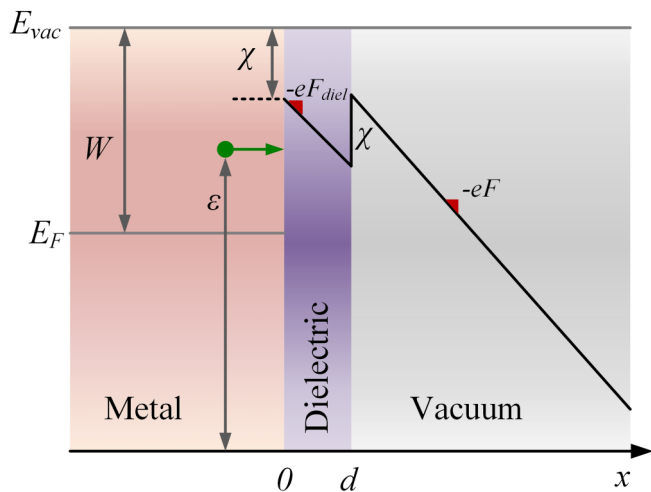


FIG. 1. Field emission from a metal surface coated with a dielectric. The metal-dielectric interface is located at $x = 0$, and the coating's thickness is d . The metal has Fermi level E_F and work function W . The dielectric has electron affinity of χ and dielectric constant of ϵ_{diel} . The electron initial longitudinal energy is ϵ . The external dc field of F (in the vacuum) is applied to the emitter surface. The field in the dielectric is $F_{\text{diel}} = F/\epsilon_{\text{diel}}$.

constant of the coating layer; and d is the thickness of the dielectric coating layer.

To calculate the probability of electron tunneling through the barrier, we solve the 1D time-independent Schrödinger equation,

$$-\frac{\hbar^2}{2m} \frac{\partial^2}{\partial x^2} \psi(x) + [V(x) - \epsilon] \psi(x) = 0, \quad (2)$$

where $\psi(x)$ is the complex electron wave function, \hbar is the reduced Planck's constant, m is the electron mass, $V(x)$ is the potential given in Eq. (1), and ϵ is the initial longitudinal energy of the electrons incident on the metal surface. Here, for simplicity, the electron mass m in all three regions (i.e., metal, dielectric, and vacuum) is set equal to the electron rest mass.

For $x < 0$, the solution to Eq. (2) is

$$\psi_I(x) = e^{ik_0x} + R_1 e^{-ik_0x}, \quad (3)$$

where $k_0 = \sqrt{2m\epsilon/\hbar^2}$, and R_1 is the reflection coefficient at the metal-dielectric interface. Equation (3) represents the superposition of an incident wave and a reflected wave.

For $0 \leq x < d$, Eq. (2) can be solved by transforming it into the form of $d^2\psi/d\eta_1^2 + \eta_1\psi = 0$ [1,41–43], and the solution is expressed in terms of Airy functions as

$$\psi_{II}(x) = a\text{Ai}(-\eta_1) + b\text{Bi}(-\eta_1), \quad (4)$$

where $\eta_1 = (\frac{2meF_{\text{diel}}}{\hbar^2})^{1/3}(x + \frac{\epsilon - V_1}{eF_{\text{diel}}})$, with $V_1 = V_0 - \chi$; Ai and Bi are the Airy functions of the first kind and second kind, respectively. ψ_{II} represents the superposition of the transmitted wave from the metal-dielectric interface and the reflected wave from the dielectric-vacuum interface.

For $x \geq d$, the Schrödinger equation, Eq. (2), is transformed into $d^2\psi/d\eta_2^2 + \eta_2\psi = 0$, whose solution is

$$\psi_{III}(x) = T_3[\text{Ai}(-\eta_2) - i\text{Bi}(-\eta_2)], \quad (5)$$

where $\eta_2 = (\frac{2meF}{\hbar^2})^{1/3}(x + \frac{\epsilon - V_2}{eF})$, with $V_2 = V_0 + e(F - F_{\text{diel}})d$. Equation (5) represents an outgoing wave traveling into the vacuum.

The imposition of the boundary conditions that ψ and $d\psi/dx$ are continuous at both the metal-dielectric interface $x = 0$ and the dielectric-vacuum interface $x = d$ gives

$$1 + R_1 = aA_1 + bB_1, \quad (6a)$$

$$1 - R_1 = \zeta(aA'_1 + bB'_1), \quad (6b)$$

$$aA_2 + bB_2 = T_3(A_3 - iB_3), \quad (6c)$$

$$aA'_2 + bB'_2 = \xi T_3(A'_3 - iB'_3), \quad (6d)$$

where $A_1 = \text{Ai}[-\eta_1(x=0)]$, $B_1 = \text{Bi}[-\eta_1(x=0)]$, $A'_1 = \text{Ai}'[-\eta_1(x=0)]$, $B'_1 = \text{Bi}'[-\eta_1(x=0)]$, $A_2 = \text{Ai}[-\eta_1(x=d)]$, $B_2 = \text{Bi}[-\eta_1(x=d)]$, $A'_2 = \text{Ai}'[-\eta_1(x=d)]$, $B'_2 = \text{Bi}'[-\eta_1(x=d)]$, $A_3 = \text{Ai}[-\eta_2(x=d)]$, $B_3 = \text{Bi}[-\eta_2(x=d)]$, $A'_3 = \text{Ai}'[-\eta_2(x=d)]$, $B'_3 = \text{Bi}'[-\eta_2(x=d)]$, Ai' and Bi' are the first derivative of Ai and Bi with respect to their arguments, $\zeta = \frac{i}{k_0}(\frac{2meF_{\text{diel}}}{\hbar^2})^{1/3}$, and $\xi = (F/F_{\text{diel}})^{1/3}$. The transmission coefficient T_3 is

$$T_3 = \frac{2}{\pi[P(U + \zeta Y) - \xi Q(V + \zeta Z)]}, \quad (7)$$

where $P = A_3 - iB_3$, $Q = A'_3 - iB'_3$, $U = A_1B'_2 - B_1A'_2$, $V = A_1B_2 - B_1A_2$, $Y = A'_1B'_2 - B'_1A'_2$, and $Z = A'_1B_2 - B'_1A_2$. Note that the heterostructure in Fig. 1 can be easily solved numerically using transfer matrix approaches [2,44]; here, we expand such a setup analytically.

The transmission probability, defined as $D(\epsilon) = J_3(\epsilon)/J_i(\epsilon)$, is the ratio of the transmitted probability current density to the incident probability current density, with probability current density $J = i\hbar/2m(\psi\nabla\psi^* - \psi^*\nabla\psi)$, given by

$$D(\epsilon) = \frac{1}{\pi} \frac{1}{k_0} \left(\frac{2meF}{\hbar^2} \right)^{1/3} |T_3|^2 = \frac{4\alpha\xi}{\pi^3} \frac{1}{\Gamma^2 + \Delta^2}, \quad (8)$$

where $\Gamma = A_3U + \alpha B_3Y - \xi(A'_3V + \alpha B'_3Z)$, and $\Delta = B_3U - \alpha A_3Y + \xi(\alpha A'_3Z - B'_3V)$, with $\alpha = |\zeta| = \frac{1}{k_0}(\frac{2meF_{\text{diel}}}{\hbar^2})^{1/3}$.

The electron emission current density can therefore be obtained by

$$J = e \int_0^\infty D(\epsilon) N(\epsilon) d\epsilon, \quad (9)$$

where $D(\epsilon)$ is given in Eq. (8) and $N(\epsilon) = \frac{mk_B T}{2\pi^2 \hbar^3} \ln[1 + \exp(\frac{E_F - \epsilon}{k_B T})]$ is the number density of electrons impinging normal to the metal surface across a unit area per unit time, which is calculated from the free electron theory of metal [2,45], with k_B the Boltzmann's constant and T the temperature.

III. PROBABILITY OF ELECTRON TUNNELING FROM DIELECTRIC COATED SURFACE

Figure 2 shows the tunneling probability for electrons with initial longitudinal energy of $\epsilon = E_F$, as a function of dielectric thickness d and dielectric constant ϵ_{diel} , under various combinations of dc electric field F and dielectric electron affinity χ , calculated from Eq. (8). The metal is assumed to be gold, with work function $W = 5.1$ eV and Fermi energy $E_F = 5.53$ eV. Unless stated otherwise, these values are the default cathode metal properties in this study. When $F = 1$

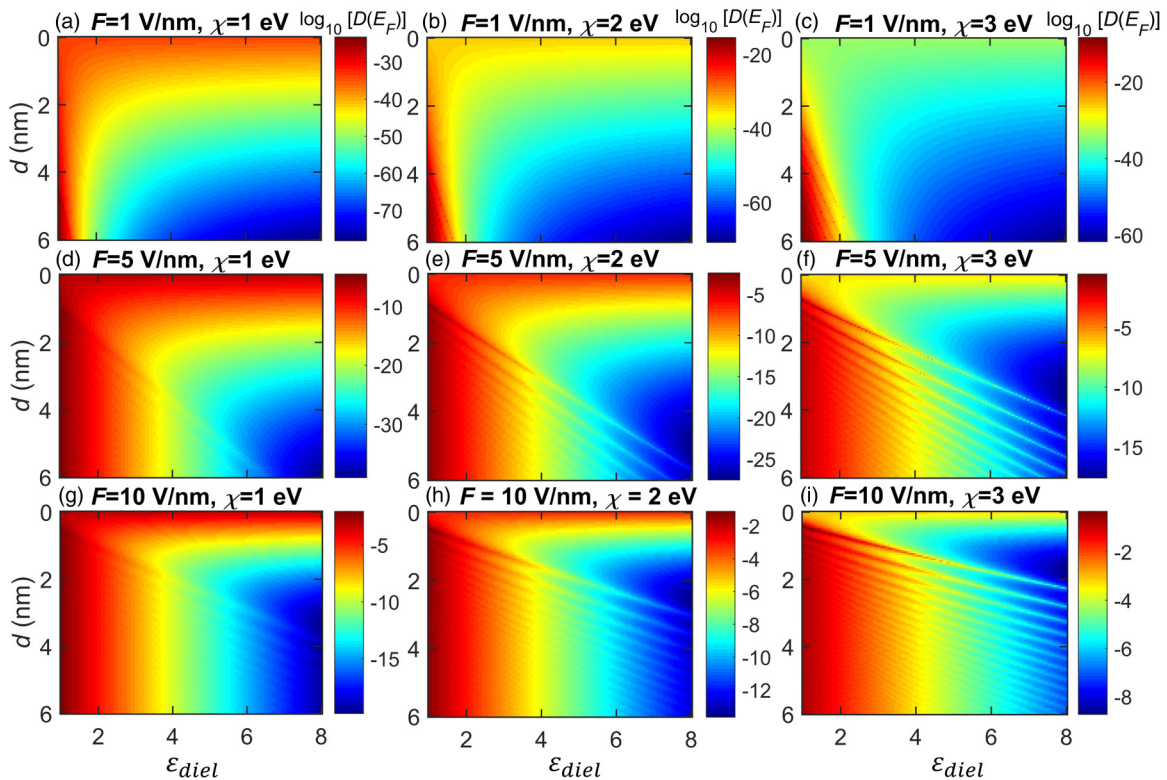


FIG. 2. Electron tunneling probability $D(\varepsilon = E_F)$ as a function of the dielectric thickness d and dielectric constant $\varepsilon_{\text{diel}}$, under various combinations of dc electric field F and the dielectric electron affinity χ : (a)–(c) $F = 1$ V/nm, (d)–(f) $F = 5$ V/nm, (g)–(i) $F = 10$ V/nm; with $\chi = 1$ eV in (a), (d), (g), $\chi = 2$ eV in (b), (e), (h), and $\chi = 3$ eV in (c), (f), (i). The electron initial longitudinal energy is assumed to be Fermi energy $\varepsilon = E_F$. The metal is assumed to be gold, with work function $W = 5.1$ eV and Fermi energy $E_F = 5.53$ eV.

V/nm, as shown in Figs. 2(a)–2(c), the electron tunneling probability $D(E_F)$ decreases with the dielectric constant $\varepsilon_{\text{diel}}$ for a given d . For $\varepsilon_{\text{diel}} > 2$, $D(E_F)$ decreases as d increases; however, for $\varepsilon_{\text{diel}} < 2$, $D(E_F)$ increases as d increases. As the dc electric field increases to $F = 5$ V/nm or $F = 10$ V/nm, as shown in Figs. 2(d)–2(i), it is obvious that the tunneling probability $D(E_F)$ increases, due to the narrowing of the surface potential barrier by the dc electric field. More importantly, there appear strong resonant peaks in $D(E_F)$. For a given F and χ , the resonant peaks shift to a larger value of $\varepsilon_{\text{diel}}$ as d increases. The resonant peaks extend to a larger area in the $d - \varepsilon_{\text{diel}}$ domain as either F or χ increases.

The effects of dielectric thickness d , dielectric constant $\varepsilon_{\text{diel}}$, and dielectric electron affinity χ on the electron tunneling probability $D(E_F)$ are further shown in line plots in Fig. 3. The solid curves, which give $D(E_F)$ as a function of d in Figs. 3(a)–3(c), show a parabolalike shape when $0 < d < d_0$, with a rough estimation of $d_0[\text{nm}] \sim \varepsilon_{\text{diel}}W/eF$. When $d > d_0$, $D(E_F)$ oscillates around a constant and the oscillation amplitude decays with d . For a given set of $\varepsilon_{\text{diel}}$ and χ as in Fig. 3(a), when F increases, the tunneling probability increases, due to the narrowing of the potential barrier by the dc electric field. The resonance peaks shift towards smaller dielectric thickness values as F increases, indicated by the dashed line in Fig. 3(a). For fixed F and χ as in Fig. 3(b), the tunneling probability decreases with increasing $\varepsilon_{\text{diel}}$, due to the smaller dc electric field $F_{\text{diel}} = F/\varepsilon_{\text{diel}}$ inside the dielectric. The dashed line in Fig. 3(b) indicates that the resonance peaks shift to a larger dielectric thickness value as $\varepsilon_{\text{diel}}$ in-

creases, which is also consistent with the rough estimation of $d_0(\text{nm}) \sim \varepsilon_{\text{diel}}W/eF$. For a given combination of F and $\varepsilon_{\text{diel}}$ as in Fig. 3(c), the tunneling probability increases with electron affinity χ , due to the lowering of the potential barrier at the metal-dielectric interface. It is shown that increasing χ makes the oscillation stronger; meanwhile, the resonance peaks slightly shift to a small dielectric thickness.

It is interesting to find that the tunneling probability from coated cathodes can be larger than that from the uncoated ones. Some specific cases are highlighted by the yellow block in Figs. 3(b) and 3(c). For these cases, the dielectric coated cathode has larger electron tunneling probability than the uncoated one, regardless of the thickness of the coating. Figures 3(b) and 3(c) show that the dielectric coating with small $\varepsilon_{\text{diel}}$ and large χ tends to enhance field emission from 1D flat cathode surfaces.

Figures 3(d)–3(f) show $D(E_F)$ as a function of $\varepsilon_{\text{diel}}$ for various F , d , and χ . It is obvious that the tunneling probability decreases with dielectric constant, for a given combination of F , d , and χ , due to the smaller dc electric field inside the dielectric. For fixed F and χ in Fig. 3(e), as d increases, there appear more resonance peaks for $D(E_F)$ as a function of $\varepsilon_{\text{diel}}$. The curves for dielectric thickness $d > 2$ nm start to overlap. That is because $D(E_F)$ gradually becomes constant against d for a given combination of $\varepsilon_{\text{diel}}$, χ , and F , which has been shown in Figs. 3(a)–3(c). Increasing χ results in more and stronger resonance peaks on curves for $D(E_F)$ vs $\varepsilon_{\text{diel}}$, and extends those resonance peaks to large $\varepsilon_{\text{diel}}$ values, as shown in Fig. 3(f).

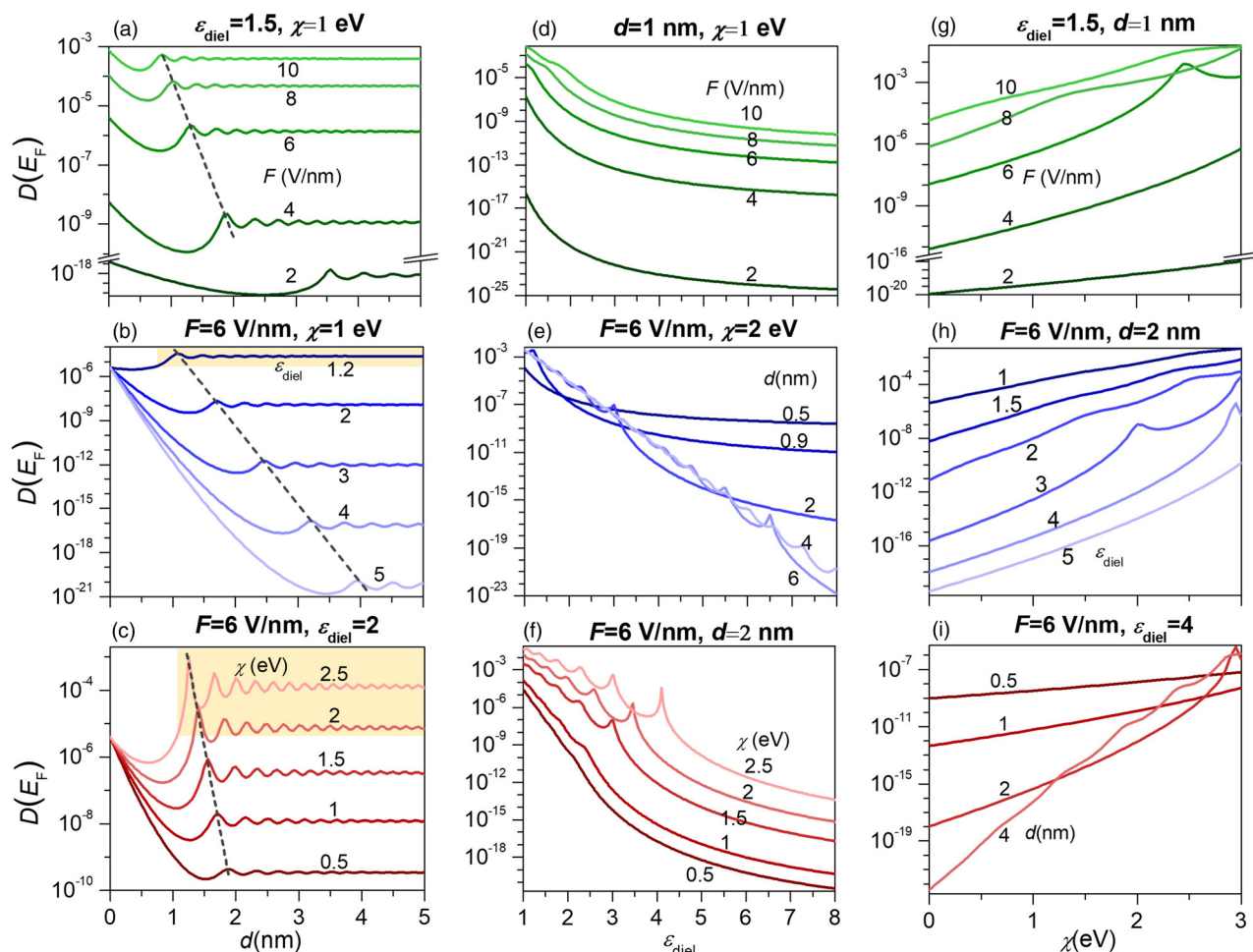


FIG. 3. Effects of dielectric thickness d , dielectric constant ϵ_{diel} , dielectric electron affinity χ , and dc electric field F on the electron tunneling probability $D(\epsilon = E_F)$ from dielectric coated metal surface. $D(\epsilon = E_F)$, calculated from Eq. (8), as a function of (a)–(c) dielectric thickness d ; (d)–(f) dielectric constant ϵ_{diel} ; and (g)–(i) dielectric electron affinity χ . The electron initial energy is assumed to be Fermi level E_F . The metal is assumed to be gold, with work function $W = 5.1$ eV and Fermi energy $E_F = 5.53$ eV.

$D(E_F)$ as a function of χ is shown in Figs. 3(g)–3(i) for various F , ϵ_{diel} , and d . The tunneling probability increases with χ , for a given set of F , ϵ_{diel} , and d , due to the lowering of the potential barrier at the metal-dielectric interface. When ϵ_{diel} increases, $D(E_F)$ decreases, as shown in Fig. 3(h), due to the smaller dc electric field inside the dielectric and therefore wider potential barrier for an electron to tunnel through. When $F = 6$ V/nm and $\epsilon_{\text{diel}} = 4$ in Fig. 3(i), the slope of the curves increases with d . It can be observed that the tunneling probability for cases of $d = 2$ nm and 4 nm are larger than that for cases of $d = 0.5$ nm and 1 nm for larger χ , which has also been shown in Figs. 3(a)–3(c). Additionally, more resonance peaks are observed on curves for $D(E_F)$ as a function of χ , when d increases.

Figure 4(a) shows the electron tunneling probability $D(\epsilon)$ as a function of electron initial longitudinal energy ϵ , for various combinations of dielectric coating thickness d , dielectric constant ϵ_{diel} , and electron affinity χ , with the applied dc electric field $F = 7$ V/nm. The tunneling probability increases as ϵ becomes larger, due to the lower potential barrier seen by

electrons with larger ϵ . Resonances appear at certain electron initial longitudinal energies, e.g., at $\epsilon \approx E_F$, 7 eV, and 9 eV for the case of $d = 1$ nm, $\epsilon_{\text{diel}} = 1.5$, and $\chi = 2$ eV [orange curve in Fig. 4(a)]. It is interesting to note that similar resonance behavior is also observed in previous studies in electron tunneling through the metal-oxide-semiconductor structures [46], double-barrier semiconductors [47], metal surfaces with closely positioned positive ions [48], and nanostructured semiconductor film cathodes [49]. Figure 4(b) shows the electron emission current density per energy $J(\epsilon) = eN(\epsilon)D(\epsilon)$ as a function of ϵ for three temperatures at $T = 100, 300$, and 2000 K. It is obvious that when $T = 2000$ K, more electrons with initial energies above the Fermi level are emitted, since more electrons are populated above the Fermi level at higher temperature. The contribution due to thermionic emission (i.e., emission of electrons with ϵ above the vacuum level) can be observed for $T = 2000$ K, as indicated in the red shaded area. The total emission current density [calculated from Eq. (9)] is $J = 3389, 3497$, and 21150 A/cm² at $T = 100, 300$, and 2000 K, respectively.

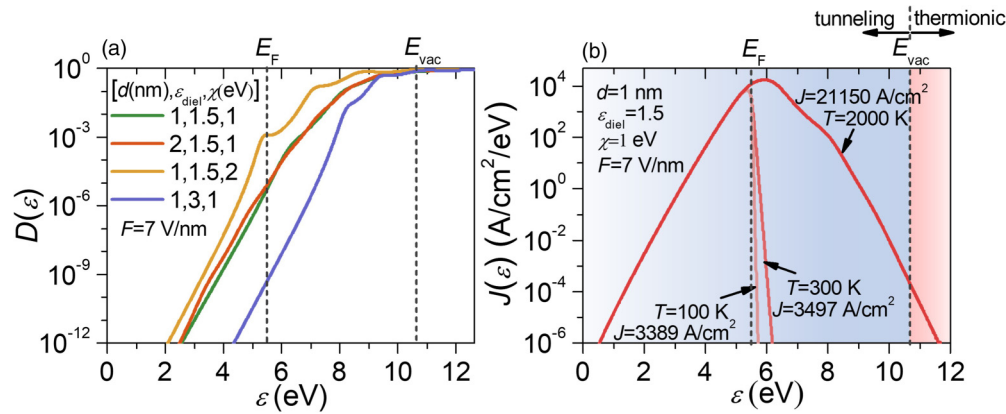


FIG. 4. (a) Electron tunneling probability $D(\epsilon)$ as a function of electron initial longitudinal energy ϵ , for various combinations of dielectric thickness d , dielectric constant ϵ_{diel} , and electron affinity χ , at the applied dc field of 7 V/nm; (b) the emission current density per energy $J(\epsilon) = eN(\epsilon)D(\epsilon)$ under various temperatures $T = 100, 300,$ and 2000 K, for fixed $d = 1$ nm, $\epsilon_{\text{diel}} = 1.5$, $\chi = 1$ eV, and $F = 7$ V/nm.

IV. EMISSION CURRENT DENSITY FROM DIELECTRIC COATED METAL SURFACE

Figure 5 shows effects of dielectric thickness d , dielectric constant ϵ_{diel} , electron affinity χ , and dc electric field F on the

emission current density J calculated from Eq. (9). Since most of the emitted electrons are with initial energies near the Fermi level at room temperature, indicated in Fig. 4(b), the emission current density follows similar trends as the tunneling

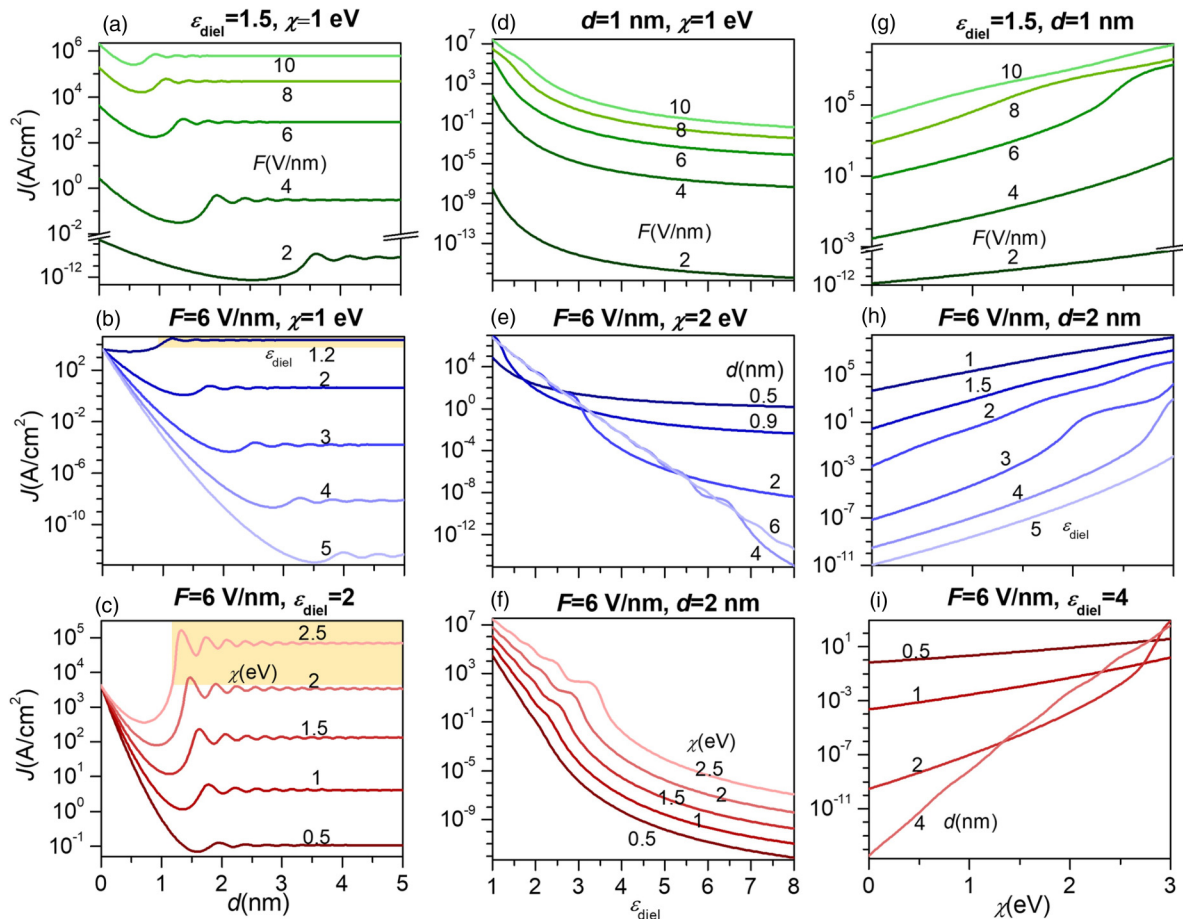


FIG. 5. Effects of dielectric thickness d , dielectric constant ϵ_{diel} , dielectric electron affinity χ , and dc electric field F on the electron emission current density from dielectric coated metal surface. The electron emission current density, calculated from Eq. (9), as a function of (a)–(c) dielectric thickness d ; (d)–(f) dielectric constant ϵ_{diel} ; and (g)–(i) dielectric electron affinity χ . The metal is assumed to be gold, with work function $W = 5.1$ eV and Fermi energy $E_F = 5.53$ eV.

probability $D(E_F)$ in Fig. 3. The emission current density, as a function of dielectric thickness, shows a parabolalike shape in the range of $0 < d \lesssim d_0[\text{nm}] = \varepsilon_{\text{diel}}W/eF$. When $d \gtrsim d_0$, J oscillates around a constant. The behavior where the emission current density settles to a constant value for thick dielectric coatings under a fixed electric field is because the potential in the vacuum region drops below the electron initial energy, which does not contribute to the potential barrier for electron tunneling. As a result, the emission current is determined by the barrier inside the dielectric region only and does not depend on the dielectric thickness, when the thickness is large. The oscillation can be ascribed to the interference between incident electron waves and reflected waves inside the dielectric layer [46]. It is found that resonance peaks on the curves for emission current density J in Fig. 5 are not as sharp as those on electron tunneling probability $D(E_F)$ in Fig. 3. This can be explained by the emission of electrons with different initial energies, which, in combination, smooths the curve. The possible physical cause is the broadening of the resonances associated with the interference between reflected and transmitted waves for different initial energy of the electrons [44]. As F increases, the emission current density increases, and resonance peaks shift towards smaller dielectric thickness d , as shown in Fig. 5(a). When the dielectric constant $\varepsilon_{\text{diel}}$ increases, the emission current density becomes smaller due to the smaller dc electric field in the dielectric, so that the barrier inside the dielectric is less narrowed. Meanwhile, an increased $\varepsilon_{\text{diel}}$ shifts the resonance peaks to a large thickness d , as shown in Fig. 5(b). When the electron affinity χ of the dielectric increases, the emission current density increases because of the lowering of the potential barrier at the metal-dielectric interface, and resonance peaks shift slightly to small thickness values. Similar to the tunneling probability in Fig. 3, a relatively small $\varepsilon_{\text{diel}}$ or a larger χ may induce a larger emission current density than the bare metal, as highlighted by the yellow blocks in Figs. 5(b) and 5(c). For the case of $F = 6 \text{ V/nm}$, $\varepsilon_{\text{diel}} = 2$, and $\chi = 2 \text{ eV}$ in Fig. 5(c), J is larger than that of the uncoated case only near a few resonant peaks, whereas $D(E_F)$ for this case in Fig. 3(c) is almost continuously larger than the uncoated case for $d > 1.5 \text{ nm}$. It can be explained by the fact that more electrons are emitted with initial longitudinal energies below Fermi level at room temperature, as shown in Fig. 4(b). For electrons with $\varepsilon < E_F$, the tunneling probability from coated metals with dielectric thickness d highlighted in Fig. 3(c) can be smaller than that from bare metal, thus yielding a smaller overall emission current density.

The electron emission current density J as a function of dielectric constant $\varepsilon_{\text{diel}}$ is shown in Figs. 5(d)–5(f). When $\varepsilon_{\text{diel}}$ increases, J decreases. As shown in Fig. 5(e), for the case of $F = 6 \text{ V/nm}$ and $\chi = 2 \text{ eV}$, the curves for $d > 2 \text{ nm}$ start to get overlapped, since the emission current density becomes almost constant as d becomes large, as shown in Figs. 5(a)–5(c). When χ increases in Fig. 5(f), more resonance peaks appear and extend towards larger values of $\varepsilon_{\text{diel}}$.

Figures 5(g)–5(i) show the electron emission current density as a function of dielectric electron affinity χ . When χ increases, the emission current density increases. There is a sharp increase of the slope at $\chi \approx 2.5 \text{ eV}$ for $F = 6 \text{ V/nm}$ in Fig. 5(g). The sharp increases of the slope are also shown in Fig. 5(h) at $\chi \approx 1.8 \text{ eV}$ and $\chi \approx 2.8 \text{ eV}$ for the case of

$\varepsilon_{\text{diel}} = 3$, and at $\chi \approx 2.6 \text{ eV}$ for the case of $\varepsilon_{\text{diel}} = 4$. These features are consistent with the resonant peaks of $D(E_F)$ observed in Figs. 3(g) and 3(h). When the dielectric thickness increases, the slope of the curves in Fig. 5(i) increases. At $\chi = 3 \text{ eV}$, the emission current density with $d = 2$ and 4 nm exceeds that with $d = 0.5$ and 1 nm in Fig. 5(i). This shows that at large χ surfaces with thicker dielectric become better emitters, which is because a higher χ would lower the surface barrier, and a thicker dielectric layer would provide an overall smaller tunneling barrier (see, e.g., the barriers in Fig. 7).

As already seen in Figs. 3 and 5, coating with a relatively small $\varepsilon_{\text{diel}}$ or a larger χ may induce a larger emission current density than the uncoated cathode. Figure 6 provides more calculations to determine the threshold values of dielectric thickness d_{th} and dielectric constant $\varepsilon_{\text{diel}}^{\text{th}}$, at which the emission current density J is equal to that from the bare metal, for a given dielectric electron affinity χ and dc electric field F . When $\chi = 1 \text{ eV}$ and $F = 5 \text{ V/nm}$, the thresholds are found to be $d_{\text{th}} = 1.5 \text{ nm}$ and $\varepsilon_{\text{diel}}^{\text{th}} = 1.38$, as shown in Fig. 6(a). A dielectric constant smaller than $\varepsilon_{\text{diel}}^{\text{th}}$ would enhance the electron emission compared to the uncoated case, with thicknesses corresponding to the curves above the horizontal dashed line. When the dielectric electron affinity increases to $\chi = 2 \text{ eV}$, the dielectric thickness and dielectric constant thresholds becomes larger, i.e., $d_{\text{th}} = 1.77 \text{ nm}$ and $\varepsilon_{\text{diel}}^{\text{th}} = 2.09$ in Fig. 6(b). When the dc field increases to 10 V/nm , the dielectric thickness and dielectric constant threshold shift towards smaller values, i.e., $d_{\text{th}} = 0.86 \text{ nm}$ and $\varepsilon_{\text{diel}}^{\text{th}} = 1.35$ in Fig. 6(c). Although it is difficult to give an exact expression to determine the dielectric constant and thickness thresholds, it is found that all three cases in Fig. 6 roughly follow the empirical relation at room temperature,

$$d_{\text{th}}[\text{nm}] = \frac{\varepsilon_{\text{diel}}^{\text{th}}W}{eF}, \quad (10)$$

whose physical origin will become clear from the analysis of the potential barrier profiles in Fig. 7.

Figures 7(a)–7(c) show the potential profile induced by the dc electric field $F = 5 \text{ V/nm}$, for the coated metal with various dielectric thicknesses. The dielectric constants for Figs. 7(a)–7(c) are $\varepsilon_{\text{diel}} = 1.2, 1.38$, and 1.5 , respectively, where $\varepsilon_{\text{diel}} = 1.38$ is the dielectric constant threshold for the case of $\chi = 1 \text{ eV}$ and $F = 5 \text{ V/nm}$ in Fig. 6(a). In the dielectric layer, the slope of the potential profile is $F/\varepsilon_{\text{diel}}$. To evaluate how the potential barrier affects the tunneling probability, the potential barrier width $w(\varepsilon)$, indicated by the double-arrow line at initial energy ε in Fig. 7(a), and the corresponding tunneling probability $D(\varepsilon)$ at $\varepsilon = E_F$ are plotted as a function of dielectric thickness d in Figs. 7(d)–7(f). The potential barrier width $w(E_F)$ increases with the dielectric thickness d when $d < \varepsilon_{\text{diel}}(W - \chi)/eF$ [for arbitrary ε , this is $\varepsilon_{\text{diel}}(W + E_F - \varepsilon - \chi)/eF$], due to the smaller electric field in the dielectric than that in the vacuum. $w(E_F)$ decreases in the dielectric thickness range of $\varepsilon_{\text{diel}}(W - \chi)/eF < d < \varepsilon_{\text{diel}}W/eF$, where electrons need to tunnel through two separate barriers—one in the dielectric and the other in the vacuum. When $d > \varepsilon_{\text{diel}}W/eF$ [this is $\varepsilon_{\text{diel}}(W + E_F - \varepsilon)/eF$ for arbitrary ε], electrons with initial longitudinal energy of E_F can be emitted by tunneling through only the barrier in the

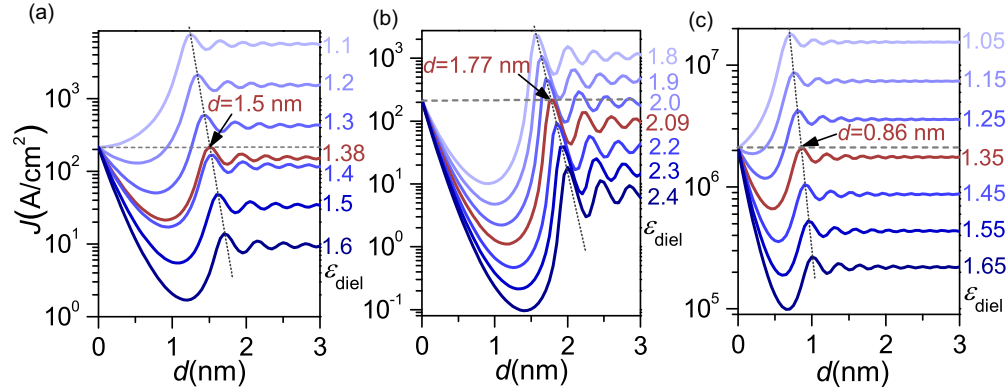


FIG. 6. Emission current density as a function of dielectric thickness d under various dielectric constants ϵ_{diel} for (a) $\chi = 1$ eV and $F = 5$ V/nm, (b) $\chi = 2$ eV and $F = 5$ V/nm, and (c) $\chi = 1$ eV and $F = 10$ V/nm. The metal is assumed to be gold, with work function $W = 5.1$ eV and Fermi energy $E_F = 5.53$ eV.

dielectric and therefore the barrier width $w(E_F)$ reaches a constant for the same applied dc electric field.

The corresponding electron tunneling probability, shown as blue curves in Figs. 7(d)–7(f), decreases as $w(E_F)$ increases, and increases when $w(E_F)$ decreases. $D(E_F)$ reaches its first resonance peak at $d \approx \epsilon_{\text{diel}}W/eF$, where electrons only need to tunnel through one potential barrier to emit. The red dashed lines in Figs. 7(d)–7(f) indicate that the maximum resonance peak of $D(E_F)$ is roughly at the same thickness $d = \epsilon_{\text{diel}}W/eF$ [cf. Eq. (10)], where $w(E_F)$ starts to become a constant. More calculations (not shown) for various combi-

nations of F and χ show that the maximum resonance peak of $D(E_F)$ can deviate but remain close to $d = \epsilon_{\text{diel}}W/eF$. It is also found that the location of the zeros of the Airy function for the electron wave functions approximately matches with the coating thickness predicted by Eq. (10), where the maximum resonant peak occurs. The oscillation in $D(E_F)$ after the maximum is due to the interference between the incident waves and reflected wave at the dielectric-vacuum interface. It is also observed that when $\epsilon_{\text{diel}} = 1.38$, $D(E_F)$ by the coated metal with the dielectric thickness $d = \epsilon_{\text{diel}}W/eF = 1.41$ nm is larger than that by the bare metal, although the potential barrier width of the coated case is larger than that of the bare one. By observing the potential profiles in Figs. 7(a)–7(c), it is expected that the average constant value around which $D(E_F)$ oscillates at large d may be estimated by

$$D(\epsilon) = \frac{4\alpha}{\pi} \frac{1}{(A_1 + \alpha B_1')^2 + (\alpha A_1' - B_1)^2}, \quad (11)$$

with all the terms as defined in Sec. II [in Eqs. (6) and (8)], which is the electron tunneling probability due to a single triangular barrier (i.e., Fowler-Nordheim field emission [43,50]) with potential barrier height $W - \chi$ and electric field F_{diel} . Equation (11) is plotted as blue dotted lines in Figs. 7(d)–7(f).

Thus, by comparing Eq. (11) and the tunneling probability from the uncoated cathode, one may determine the threshold value of dielectric constant ϵ_{diel} , which is then used in Eq. (10) to give the threshold value of dielectric constant d_{th} , in order to have field emission current larger than the uncoated case from 1D flat surfaces.

V. COMPARISON WITH MODIFIED DOUBLE-BARRIER FOWLER-NORDHEIM EQUATION

In this section, we compare our quantum model with the modified Fowler-Nordheim (FN) equation with a double-barrier potential profile, developed for cathode surfaces with an oxidation layer [39,40],

$$J = \frac{e^3 F^2}{16\pi^2 \hbar W B^2} \exp\left[-\frac{4\sqrt{2m}}{3e\hbar F} W^{\frac{3}{2}} C\right], \quad (12)$$

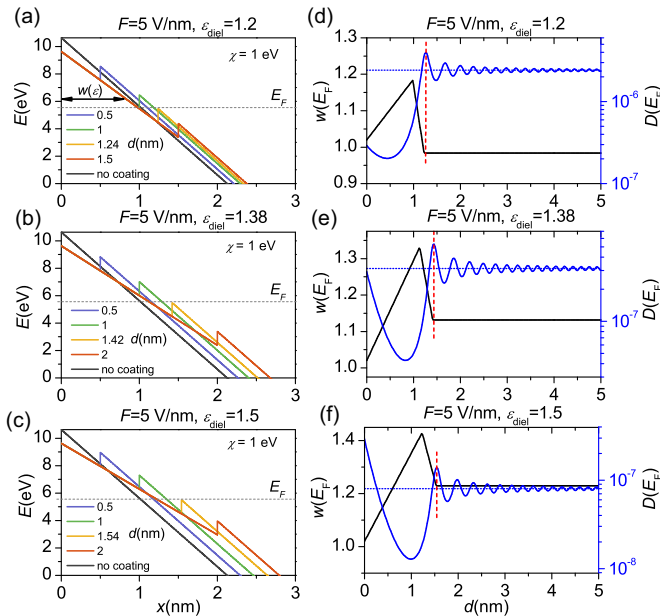


FIG. 7. (a)–(c) Potential profile for coated metal with dielectric constants of (a) $\epsilon_{\text{diel}} = 1.2$, (b) $\epsilon_{\text{diel}} = 1.38$, and (c) $\epsilon_{\text{diel}} = 1.5$ for various dielectric thicknesses d (nm). (d)–(f) Barrier width w seen by the electron with initial longitudinal energy of $\epsilon = E_F$, and the corresponding electron tunneling probability D as a function of dielectric thickness d for coatings with dielectric constants of (d) $\epsilon_{\text{diel}} = 1.2$, (e) $\epsilon_{\text{diel}} = 1.38$, and (f) $\epsilon_{\text{diel}} = 1.5$. The applied dc electric field $F = 5$ V/nm. Blue dotted lines are from Eq. (11).

with

$$B = \varepsilon_{\text{diel}} \left[\sqrt{\frac{W_{\text{eff}}}{W}} - H(W_{\text{eff}} - eF_{\text{diel}}d) \sqrt{\frac{W_{\text{eff}} - eF_{\text{diel}}d}{W}} \right] + H(W - eF_{\text{diel}}d) \sqrt{\frac{W - eF_{\text{diel}}d}{W}}, \quad (12a)$$

$$C = \varepsilon_{\text{diel}} \left[\left(\frac{W_{\text{eff}}}{W} \right)^{\frac{3}{2}} - H(W_{\text{eff}} - eF_{\text{diel}}d) \left(\frac{W_{\text{eff}} - eF_{\text{diel}}d}{W} \right)^{\frac{3}{2}} \right] + H(W - eF_{\text{diel}}d) \left(\frac{W - eF_{\text{diel}}d}{W} \right)^{\frac{3}{2}}, \quad (12b)$$

where e and m are the positive elementary charge and electron mass (set equal to electron rest mass in all three regions of metal, dielectric, and vacuum), \hbar is the reduced Planck's constant, F is the applied dc electric field in the vacuum, $F_{\text{diel}} = F/\varepsilon_{\text{diel}}$ is the electric field inside the dielectric layer, W is the nominal work function of the metal, $W_{\text{eff}} = W - \chi$ is the effective work function at the metal-dielectric interface, d is the thickness of the dielectric layer, and $H(x)$ is the Heaviside function. In case of no dielectric layer, $W_{\text{eff}} = W$, $d = 0$, $\varepsilon_{\text{diel}} = 1$, B and C become 1, and Eq. (12) recovers the Fowler-Nordheim equation [1].

The electron emission current density of the quantum model, calculated from Eq. (9), is compared with that calculated from the modified FN equation, Eq. (12), as shown in Fig. 8. The two models show good agreement in the scaling, with the quantum model giving a higher emission current density in general. This is because the quantum model considers electron emission from all the energy levels at room temperature $T = 300$ K, whereas the FN based model assumes electron emission at 0 K. The quantum model shows resonance behavior in J vs d , which cannot be revealed by the modified FN equation.

VI. CONCLUSIONS

In summary, we have developed an exact theory for field emission from dielectric coated cathode surfaces, by solving

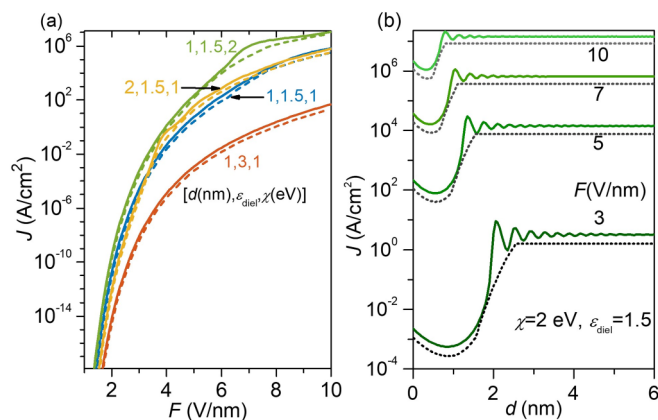


FIG. 8. (a) The emission current density J from the dielectric coated metal, calculated from Eq. (9) (solid lines), and the modified Fowler-Nordheim equation, Eq. (12) (broken lines), as a function of electric field under various combinations of dielectric thickness d , dielectric constant $\varepsilon_{\text{diel}}$, and dielectric electron affinity χ . (b) J from the dielectric coated metal, calculated from the quantum model (solid lines) and the modified Fowler-Nordheim equation (broken lines), as a function of dielectric thickness d . The dielectric has $\varepsilon_{\text{diel}} = 1.5$ and $\chi = 2$ eV.

the one-dimensional time-independent Schrödinger equation with a double-triangular barrier, which is formed by applying dc electric field to the dielectric coated cathode surface. The model includes both field emission and thermionic emission. It is found that the combination of a small dielectric constant and a large dielectric electron affinity tends to induce a larger emission current density than bare metal for 1D flat cathode surfaces, under a given dc electric field. It is found the emission current density is larger than the uncoated case when the dielectric constant is smaller than a certain value $\varepsilon_{\text{diel}}^{\text{th}}$ and the dielectric thickness is larger than the threshold value $d_{\text{th}}[\text{nm}] \approx \varepsilon_{\text{diel}} W / eF$ with $\varepsilon_{\text{diel}} < \varepsilon_{\text{diel}}^{\text{th}}$. This relation is consistent with the sharp transition of the potential barrier width in the double-triangular barrier. Our quantum model is also compared with a modified Fowler-Nordheim equation for a double-triangular barrier, showing good agreement in the scaling of the emission current. The theory provides insights for designing the emitter with higher efficiency and better stability.

Although our theory in Eqs. (1)–(9) is valid for arbitrary electric fields inside the dielectric F_{diel} and in the vacuum F , we would like to stress that the above results regarding the determination of threshold dielectric constant and thickness are applicable to 1D flat surfaces only, where electric field enhancement is not considered. When the cathode surface strongly deviates from a flat surface, e.g., sharp emitters, the local electric field enhancement has to be taken account of [35]. As the field profiles vary nonlinearly in this case, the ratio of the electric field inside the dielectric layer and in the vacuum does not simply follow $F_{\text{diel}}/F = 1/\varepsilon_{\text{diel}}$, which needs to be calculated numerically from 2D or 3D electrostatic modeling. Once the field profiles are determined, our model can be directly used to calculate the electron emission current for any shape of emitters.

In the future, our theory can be further improved by including the image charge effect and charge trapping effects due to defects in the dielectric [39]. The material defects may limit the maximum thickness of the dielectric coating one can use. It is also interesting to explore the application of the current model for dielectric coated cathodes with spatial variations on the surfaces and for emitters of finite sizes [26,35,51]. It can also be extended to include photoelectron emission [45,52] in the model, which may be used to test the validity of the simplified treatment of an effective triangular barrier for photoemission from coated surface [35]. Comparison of the resonance behaviors of tunneling from coated cathode surfaces with those of resonant tunneling diodes [44,53] may be considered in the future. Future research may also extend the theory to study the effects of coating in small gaps or tunneling junctions [54,55].

ACKNOWLEDGMENTS

The authors would like to thank Dr. Benjamin Tong Yee of Sandia National Labs for helpful discussions. This work was supported by Air Force Office of Scientific Research

(AFOSR) YIP Grant No. FA9550-18-1-0061, Office of Naval Research (ONR) YIP Grant No. N00014-20-1-2681, and Air Force Office of Scientific Research (AFOSR) Grant No. FA9550-20-1-0409.

- [1] R. H. Fowler and L. Nordheim, Electron emission in intense electric fields, *Proc. R. Soc. London, Ser. A* **119**, 173 (1928).
- [2] K. L. Jensen, *Introduction to the Physics of Electron Emission*, 1st ed. (Wiley, Hoboken, NJ, 2017).
- [3] Q. H. Wang, A. A. Setlur, J. M. Lauerhaas, J. Y. Dai, E. W. Seelig, and R. P. H. Chang, A nanotube-based field-emission flat panel display, *Appl. Phys. Lett.* **72**, 2912 (1998).
- [4] A. A. Talin, K. A. Dean, and J. E. Jaskie, Field emission displays: A critical review, *Solid State Electron.* **45**, 963 (2001).
- [5] Y. Saito, K. Hata, A. Takakura, J. Yotani, and S. Uemura, Field emission of carbon nanotubes and its application as electron sources of ultra-high luminance light-source devices, *Phys. B (Amsterdam, Neth.)* **323**, 30 (2002).
- [6] L. W. Swanson and G. A. Schwind, A review of field electron source use in electron microscopes, *Microsc. Microanal.* **11**, 864 (2005).
- [7] F. Houdellier, L. de Knoop, C. Gatel, A. Masseur, S. Mamishin, Y. Taniguchi, M. Delmas, M. Monthieux, M. J. Hÿtch, and E. Snoeck, Development of TEM and SEM high brightness electron guns using cold-field emission from a carbon nanotip, *Ultramicroscopy* **151**, 107 (2015).
- [8] S. Sun, X. Sun, D. Bartles, E. Wozniak, J. Williams, P. Zhang, and C.-Y. Ruan, Direct imaging of plasma waves using ultrafast electron microscopy, *Struct. Dyn.* **7**, 064301 (2020).
- [9] G. N. Furse, Field emission in vacuum micro-electronics, *Appl. Surf. Sci.* **215**, 113 (2003).
- [10] E. J. Radauscher, K. H. Gilchrist, S. T. Di Dona, Z. E. Russell, J. R. Piascik, J. J. Amsden, C. B. Parker, B. R. Stoner, and J. T. Glass, Improved performance of field emission vacuum micro-electronic devices for integrated circuits, *IEEE Trans. Electron Devices* **63**, 3753 (2016).
- [11] G. Cao, Y. Z. Lee, R. Peng, Z. Liu, R. Rajaram, X. Calderon-Colon, L. An, P. Wang, T. Phan, S. Sultana, D. S. Lalush, J. P. Lu, and O. Zhou, A dynamic micro-CT scanner based on a carbon nanotube field emission x-ray source, *Phys. Med. Biol.* **54**, 2323 (2009).
- [12] K. L. Jensen, Field emitter arrays for plasma and microwave source applications, *Phys. Plasmas* **6**, 2241 (1999).
- [13] D. Shiffler, T. K. Statum, T. W. Hussey, O. Zhou, and P. Mardahl, in *Modern Microwave and Millimeter Wave Power Electronics* (IEEE, Piscataway, NJ, 2005), p. 691.
- [14] D. Shiffler, M. Ruebush, M. LaCour, K. Golby, R. Umstatt, M. C. Clark, J. Luginsland, D. Zagar, and M. Sena, Emission uniformity and emission area of explosive field emission cathodes, *Appl. Phys. Lett.* **79**, 2871 (2001).
- [15] W. Tang, D. Shiffler, K. Golby, M. LaCour, and T. Knowles, Field enhancement for fiber emitters in linear and rectangular arrays, *J. Vac. Sci. Technol. B* **32**, 052202 (2014).
- [16] P. Zhang, S. B. Fairchild, T. C. Back, and Y. Luo, Field emission from carbon nanotube fibers in varying anode-cathode gap with the consideration of contact resistance, *AIP Adv.* **7**, 125203 (2017).
- [17] P. Zhang, J. Park, S. B. Fairchild, N. P. Lockwood, Y. Y. Lau, J. Ferguson, and T. Back, Temperature comparison of looped and vertical carbon nanotube fibers during field emission, *Appl. Sci.* **8**, 1175 (2018).
- [18] S. B. Fairchild, P. Zhang, J. Park, T. C. Back, D. Marincel, Z. Huang, and M. Pasquali, Carbon nanotube fiber field emission array cathodes, *IEEE Trans. Plasma Sci.* **47**, 2032 (2019).
- [19] P. Wong, P. Zhang, and J. Luginsland, Recent theory of traveling-wave tubes: A tutorial-review, *Plasma Res. Express* **2**, 023001 (2020).
- [20] J.-M. Bonard, J.-P. Salvetat, T. Stöckli, L. Forró, and A. Châtelain, Field emission from carbon nanotubes: Perspectives for applications and clues to the emission mechanism, *Appl. Phys. A* **69**, 245 (1999).
- [21] S. Yamamoto, Fundamental physics of vacuum electron sources, *Rep. Prog. Phys.* **69**, 181 (2005).
- [22] A. Evtukh, H. Hartnagel, O. Yilmazoglu, H. Mimura, and D. Pavlidis, *Vacuum Nanoelectronic Devices: Novel Electron Sources and Applications*, 1st ed. (Wiley, Chichester, West Sussex, UK, 2015).
- [23] J.-W. Han, D.-I. Moon, and M. Meyyappan, Nanoscale vacuum channel transistor, *Nano Lett.* **17**, 2146 (2017).
- [24] P. Zhang and Y. Y. Lau, Ultrafast and nanoscale diodes, *J. Plasma Phys.* **82**, 595820505 (2016).
- [25] P. Zhang, A. Valfells, L. K. Ang, J. W. Luginsland, and Y. Y. Lau, 100 years of the physics of diodes, *Appl. Phys. Rev.* **4**, 011304 (2017).
- [26] J. Lin, P. Y. Wong, P. Yang, Y. Y. Lau, W. Tang, and P. Zhang, Electric field distribution and current emission in a miniaturized geometrical diode, *J. Appl. Phys.* **121**, 244301 (2017).
- [27] L. W. Swanson and G. A. Schwind, A review of the cold-field electron cathode, in *Advances in Imaging and Electron Physics* (Elsevier, Amsterdam, 2009), Chap. 2, pp. 63–100.
- [28] X. Shao, A. Srinivasan, W. K. Ang, and A. Khurshed, A high-brightness large-diameter graphene coated point cathode field emission electron source, *Nat. Commun.* **9**, 1288 (2018).
- [29] D. Ye, S. Moussa, J. D. Ferguson, A. A. Baski, and M. S. El-Shall, Highly efficient electron field emission from graphene oxide sheets supported by nickel nanotip arrays, *Nano Lett.* **12**, 1265 (2012).
- [30] A. T. T. Koh, Y. M. Foong, Z. Yusop, M. Tanemura, and D. H. C. Chua, Low temperature direct of graphene onto metal nano-Spindt tip with applications in electron emission, *Adv. Mater. Interfaces* **1**, 1300147 (2014).
- [31] F. Liu, N. A. Moody, K. L. Jensen, V. Pavlenko, C. W. Narvaez Villarrubia, A. D. Mohite, and G. Gupta, Single layer graphene protective gas barrier for copper photocathodes, *Appl. Phys. Lett.* **110**, 041607 (2017).

- [32] C. Henkel, R. Zierold, A. Kommini, S. Haugg, C. Thomason, Z. Aksamija, and R. H. Blick, Resonant tunneling induced enhancement of electron field emission by ultra-thin coatings, *Sci. Rep.* **9**, 6840 (2019).
- [33] L. W. Swanson and R. W. Strayer, Field-electron-microscopy studies of cesium layers on various refractory metals: Work function change, *J. Chem. Phys.* **48**, 2421 (1968).
- [34] S. B. Fairchild, T. C. Back, P. T. Murray, M. M. Cahay, and D. A. Shiffler, Low work function CsI coatings for enhanced field emission properties, *J. Vac. Sci. Technol. A* **29**, 031402 (2011).
- [35] X. Xiong, Y. Zhou, Y. Luo, X. Li, M. Bosman, L. K. Ang, P. Zhang, and L. Wu, Plasmon-enhanced resonant photoemission using atomically thick dielectric coatings, *ACS Nano* **14**, 8806 (2020).
- [36] M. Morita and T. Ohmi, Characterization and control of native oxide on silicon, *Jpn. J. Appl. Phys.* **33**, 370 (1994).
- [37] G. Wang, P. Yang, N. A. Moody, and E. R. Batista, Overcoming the quantum efficiency-lifetime tradeoff of photocathodes by coating with atomically thin two-dimensional nanomaterials, *npj 2D Mater Appl.* **2**, 17 (2018).
- [38] N. A. Moody, K. L. Jensen, A. Shabaev, S. G. Lambrakos, J. Smedley, D. Finkenstadt, J. M. Pietryga, P. M. Anisimov, V. Pavlenko, E. R. Batista, J. W. Lewellen, F. Liu, G. Gupta, A. Mohite, H. Yamaguchi, M. A. Hoffbauer, and I. Robel, Perspectives on Designer Photocathodes for X-ray Free-Electron Lasers: Influencing Emission Properties with Heterostructures and Nanoengineered Electronic States, *Phys. Rev. Appl.* **10**, 047002 (2018).
- [39] Q. Huang, Instability of field emission from silicon covered with a thin oxide due to electron trapping, *J. Appl. Phys.* **79**, 3703 (1996).
- [40] P. D. Keathley, A. Sell, W. P. Putnam, S. Guerrero, L. Velásquez-García, and F. X. Kärtner, Strong-field photoemission from silicon field emitter arrays, *Ann. Phys. (Leipzig, Germany)* **525**, 144 (2013).
- [41] W. W. Lui and M. Fukuma, Exact solution of the Schrodinger equation across an arbitrary one-dimensional piecewise-linear potential barrier, *J. Appl. Phys.* **60**, 1555 (1986).
- [42] K. F. Brennan and C. J. Summers, Theory of resonant tunneling in a variably spaced multiquantum well structure: An Airy function approach, *J. Appl. Phys.* **61**, 614 (1987).
- [43] P. Zhang and T. Pan, Exact analytical theory for inverse tunneling of free vacuum electrons into a solid, *AIP Adv.* **7**, 065307 (2017).
- [44] K. L. Jensen, D. Finkenstadt, A. Shabaev, S. G. Lambrakos, N. A. Moody, J. J. Petillo, H. Yamaguchi, and F. Liu, A photoemission moments model using density functional and transfer matrix methods applied to coating layers on surfaces: Theory, *J. Appl. Phys.* **123**, 045301 (2018).
- [45] Y. Zhou and P. Zhang, A quantum model for photoemission from metal surfaces and its comparison with the three-step model and Fowler–DuBridge model, *J. Appl. Phys.* **127**, 164903 (2020).
- [46] J. Maserjian and N. Zamani, Behavior of the Si/SiO₂ interface observed by Fowler-Nordheim tunneling, *J. Appl. Phys.* **53**, 559 (1982).
- [47] L. L. Chang, L. Esaki, and R. Tsu, Resonant tunneling in semiconductor double barriers, *Appl. Phys. Lett.* **24**, 593 (1974).
- [48] X. Tan, P. Rumbach, N. Griggs, K. L. Jensen, and D. B. Go, Theoretical analysis of 1D resonant tunneling behavior in ion-enhanced cold field and thermo-field emission, *J. Appl. Phys.* **120**, 213301 (2016).
- [49] R.-Z. Wang, W. Zhao, and H. Yan, Generalized mechanism of field emission from nanostructured semiconductor film cathodes, *Sci. Rep.* **7**, 43625 (2017).
- [50] J. W. Gadzuk and E. W. Plummer, Field emission energy distribution (FEED), *Rev. Mod. Phys.* **45**, 487 (1973).
- [51] J. B. Gunnarsson, K. Torfason, A. Manolescu, and A. Valfells, Space-charge limited current from a finite emitter in nano- and microdiodes, *IEEE Trans. Electron Devices* **68**, 342 (2021).
- [52] P. Zhang and Y. Y. Lau, Ultrafast strong-field photoelectron emission from biased metal surfaces: Exact solution to time-dependent Schrödinger equation, *Sci. Rep.* **6**, 19894 (2016).
- [53] P. J. Price, Resonant wavefunctions and exchange effect in nanostructures, *Superlattices Microstruct.* **26**, 363 (1999).
- [54] P. Zhang, Scaling for quantum tunneling current in nano- and subnano-scale plasmonic junctions, *Sci. Rep.* **5**, 9826 (2015).
- [55] S. Banerjee and P. Zhang, A generalized self-consistent model for quantum tunneling current in dissimilar metal-insulator-metal junction, *AIP Adv.* **9**, 085302 (2019).